THYROID
Volume 24, Number 4, 2014

DOI: 10.1089/thy.2013.0483

The Next Generation of Orthotopic Thyroid Cancer Models: Immunocompetent Orthotopic Mouse Models of BRAF^{V600E}-Positive Papillary and Anaplastic Thyroid Carcinoma

Pierre Vanden Borre,[1] David G. McFadden,[2] Viswanath Gunda,[1] Peter M. Sadow,[1] Shohreh Varmeh,[1] Maria Bernasconi,[1] Tyler Jacks,[3] and Sareh Parangi[1]

Background: While the development of new treatments for aggressive thyroid cancer has advanced in the last 10 years, progress has trailed headways made with other malignancies. A lack of reliable authenticated human cell lines and reproducible animal models is one major roadblock to preclinical testing of novel therapeutics. Existing xenograft and orthotopic mouse models of aggressive thyroid cancer rely on the implantation of highly passaged human thyroid carcinoma lines in immunodeficient mice. Genetically engineered models of papillary and undifferentiated (anaplastic) thyroid carcinoma (PTC and ATC) are immunocompetent; however, slow and stochastic tumor development hinders high-throughput testing. Novel models of PTC and ATC in which tumors arise rapidly and synchronously in immunocompetent mice would facilitate the investigation of novel therapeutics and approaches.

Methods: We characterized and utilized mouse cell lines derived from PTC and ATC tumors arising in genetically engineered mice with thyroid-specific expression of endogenous *Braf*$^{V600E/WT}$ and deletion of either *Trp53* (*p53*) or *Pten*. These murine thyroid cancer cells were transduced with luciferase- and GFP-expressing lentivirus and implanted into the thyroid glands of immunocompetent syngeneic B6129SF1/J mice in which the growth characteristics were assessed.

Results: Large locally aggressive thyroid tumors form within one week of implantation. Tumors recapitulate their histologic subtype, including well-differentiated PTC and ATC, and exhibit CD3+, CD8+, B220+, and CD163+ immune cell infiltration. Tumor progression can be followed *in vivo* using luciferase and *ex vivo* using GFP. Metastatic spread is not detected at early time points.

Conclusions: We describe the development of the next generation of murine orthotopic thyroid cancer models. The implantation of genetically defined murine BRAF-mutated PTC and ATC cell lines into syngeneic mice results in rapid and synchronous tumor formation. This model allows for preclinical investigation of novel therapeutics and/or therapeutic combinations in the context of a functional immune system.

Introduction

With an estimated 60,000 new cases to be diagnosed in the United States in 2013 and incidence on a dramatic rise, thyroid cancer is both common and escalating (1,2). While highly effective for the treatment of papillary thyroid cancer (PTC), traditional therapies, including surgery and radioactive iodine, are ineffective against advanced radioactive iodine-resistant PTC and undifferentiated (anaplastic) thyroid carcinoma (ATC). Approximately 45% of PTCs and 20–40% of ATCs harbor a transversion point mutation (1799T > A) in the *BRAF* gene, resulting in a valine-to-glutamate substitution at amino acid 600 of the protein (BRAF^{V600E}) and ultimately a constitutively active kinase (3,4). While true that BRAF^{V600E} plays a critical role in tumor behavior, it is also clear that not all patients with BRAF-mutant tumors have clinically aggressive thyroid cancer (5,6). Other known and putatively undiscovered gene pathways and immune factors interact with mutant BRAF signaling and contribute to the development of aggressive

[1]Department of Surgery, Massachusetts General Hospital, Harvard Medical School, Boston, Massachusetts.
[2]Thyroid Unit, Department of Medicine, Massachusetts General Hospital, Boston, Massachusetts.
[3]Koch Institute for Integrative Cancer Research and Department of Biology, Massachusetts Institute of Technology, Cambridge, Massachusetts.

characteristics in thyroid tumors. Among the additional genetic events identified to drive dedifferentiation and tumor progression are mutations affecting the tumor suppressor p53 and the PI3K-AKT pathway (5). The inactivation of p53 is detected in the vast majority of ATC (7). Though less prevalent than mutations of p53, the inactivation of the tumor suppressor PTEN leads to the activation of the PI3K-AKT pathway and is observed in ~15% of cases of ATC (8). Further, additional relevant signaling pathways and driver mutations will putatively be discovered by large-scale efforts such as The Cancer Genome Atlas (http://tcga-data.nci.nih.gov/tcga/). Mouse models have proven very useful for studying thyroid cancer progression. Both PTC and the more aggressive and lethal form of thyroid cancer, ATC, have been faithfully modeled in mice using orthotopic and, more recently, genetically engineered approaches. Each of these approaches has both advantages and disadvantages.

Our laboratory has previously shown that $BRAF^{V600E}$ plays an important role in the aggressive behavior of thyroid cancer cells and that targeted pharmaceutical inhibition of $BRAF^{V600E}$ results in impressive decreases in tumor volume and metastasis in an orthotopic animal model of ATC (6,9–12). Orthotopic placement of human thyroid cancer cell lines in the native thyroid gland is simple and inexpensive and allows metastatic spread; however, the animals are imperatively immunodeficient to prevent rejection of the human cells. Orthotopic implantation can be performed on a large number of mice allowing homogeneous cohorts of tumor-bearing animals, which are useful for investigating potential therapeutics. This model has proven useful in preclinical testing of BRAF inhibitors in the treatment of thyroid cancer and contributed to the initiation of a phase I clinical trial of vemurafenib, a selective $BRAF^{V600E}$ inhibitor, in patients with advanced thyroid cancer (3,9–11). While very practical and valuable, the absence of a functional immune system in these models unfortunately precludes the study of the native immune response to tumorigenesis and tumor progression in the presence of mutated BRAF.

Genetically engineered models are immunocompetent and elegant in their basic approach with exquisite control of genetic initiating events and timing of tumor development. However, tumors often take months to develop and therapeutic studies require sizeable cohorts of animals with tumors of similar sizes, making use of these elegant genetically engineered models for preclinical testing time-consuming, expensive, and ultimately challenging. The first transgenic model of $BRAF^{V600E}$-positive PTC was developed by overexpression of oncogenic BRAF using the thyroid-specific bovine thyroglobulin promoter (13). These mice developed well-differentiated PTC, and some transitioned to a more poorly differentiated state over 5 months. Since this initial transgenic overexpression model, PTC tumors have been generated by Cre-mediated expression of $Braf^{V600E}$ from the endogenous *Braf* locus in the thyroid gland. PTC develops in young mice (approximately five weeks of age) when $BRAF^{V600E}$ expression is induced in the embryo by crossing $Braf^{tm1Rima}$ mice to transgenic mice expressing constitutive thyroid-specific Cre recombinase (14) and in adult mice (six months after induction of BRAF expression) by crossing $Braf^{tm1Mmcm}$ mice with tamoxifen-dependent thyroid-specific CreER transgenic mice (15). PTC tumors have been rapidly induced (within one week) in adult mice by doxycycline treatment to drive doxycycline-inducible transgenic expression of $BRAF^{V600E}$, though continuous drug administration is required (14–16). A genetically engineered model of ATC has been generated in immunocompetent mice by knocking out both *p53* and *Pten*. Approximately 75% of these double-knockout mice develop follicular thyroid carcinoma that progresses to dedifferentiated ATC characterized by pleomorphism, aneuploidy, and epithelial-to-mesenchymal transition by 9 months of age (17). Given the timeframe and stochastic nature at which these mice develop tumors, it was suggested that acquired mutations spontaneously arose, though alterations were not found in various mutation hotspots, including those within the *Braf* locus (17).

A model of $BRAF^{V600E}$-positive ATC was recently developed by inducing thyroid-specific expression of $Braf^{V600E}$ from the endogenous locus along with biallelic thyroid-specific deletion of either *p53* or *Pten* (18). These novel mice develop either PTC or ATC. In this study, we utilized cell lines derived from tumors arising in this genetically engineered model for orthotopic implantation into syngeneic mice. In this ''best of both worlds'' approach, murine cell lines with well-defined genetic changes known to be important in thyroid cancer were implanted orthotopically into the thyroid environment of immunocompetent mice. This approach, which results in rapid tumor development, allows for the generation of cohorts suitable for preclinical investigation in the context of a functional immune system, thereby meeting the needs for studying the interaction of tumor cells, the tumor microenvironment, and the immune system.

Materials and Methods

Cell lines

The murine cell lines (TBP-3868, TBP-3743, TBPt-3403, and TBPt-3610R) were cultured from autochthonous tumors with either PTC-like or ATC-like pathologic features (18). In brief, TPOCreER; $Braf^{tm1Mmcm/WT}$ mice (B6129F1/J) with either homozygous floxed *p53* alleles ($Trp53^{tm1Brn/tm1Brn}$) or biallelic floxed *Pten* alleles ($Pten^{tm1Hwu/tm1Hwu}$) were treated with tamoxifen to induce thyroid-specific expression of Cre recombinase resulting in the expression of $Braf^{V600E}$ from the endogenous *Braf* promoter and the deletion of either *p53* or *Pten* (18). In addition, human 8505c ATC cells (Deutsche Sammlung von Mikroorganismen und Zellkulturen) and human BCPAP PTC cells (previously provided by Dr. G. Damante of the University of Udine, Italy) were used. All cells were maintained in Dulbecco's modified Eagle's medium supplemented with 10% fetal bovine serum and penicillin/streptomycin and incubated at 37°C with 5% CO_2.

Lentiviral transduction

The murine thyroid cancer cell lines were transduced with lentiviral vectors encoding luciferase and GFP in order to detect the primary tumor and metastases. HEK-293 cells were cotransfected with a lentiviral plasmid encoding firefly luciferase (pLenti CMV Puro LUC, w168-1) obtained from Addgene, a lentiviral plasmid encoding GFP (HIV-U6-GL3B-GFP) kindly provided by Carmelo Nucera, Beth Israel Deaconess Medical Center, and the VSVg and Δ8.9 packaging vectors using Attractene (Qiagen, Valencia, CA). The medium

was collected 24 and 48 hours after transfection and filtered with 0.44 μm Millex-HP PES filters. The murine lines (TBP-3868, TBP-3743, TBPt-3403, and TBPt-3610R) were grown to 40–60% confluence and infected with the filtered medium for 16 hours in the presence of 8 μg/mL polybrene (Sigma, St. Louis, MO). The infected cells were treated with 1–3 μg/mL puromycin before sorting for GFP-positive cells by flow cytometry using equivalent gating (MoFlo/FACSAria Sorting; Beckman Coulter, Fullerton, CA).

Tumor implantation

To determine tumor take and metastatic potential in our orthotopic models, we implanted the $BRAF^{V600E}$-positive murine tumor cell lines in the thyroid glands of syngeneic mice, as previously described (12). In brief, B6129SF1/J mice were anesthetized with 2.0–2.5% isoflurane, 100 mg/kg ketamine, and 10 mg/kg xylazine with 0.1 mg/kg buprenorphine preemptive analgesic. The thyroid gland was exposed and 10^4, 10^5, or 10^6 cells suspended in 10 μL serum-free media were unilaterally injected into the left thyroid gland of each mouse using a Hamilton syringe attached to a 27-gauge needle. The right side of the thyroid gland was not manipulated and was used as an internal control. Mice were euthanized and tumor volume was calculated as $(\pi/6) \times \text{length} \times \text{width} \times \text{height}$ (19). Prism (GraphPad Software, San Diego, CA) was utilized for statistical analysis of tumor volumes. Statistical difference was determined with one-way analysis of variance followed by the Tukey *post hoc* multiple comparison test, and p-values < 0.05 were considered significant. All animal work was done at Massachusetts General Hospital (Harvard Medical School) in accordance with federal, local, and institutional guidelines.

Bioluminescence and GFP imaging

Luciferase activity was detected in mice anesthetized with CO_2 and injected with luciferin with IVIS Imaging System 100 (Perkin Elmer, Waltham, MA). GFP fluorescence was detected using a multispectral fluorescence scanner (CRi Maestro 500, Woburn, MA) able to detect and image fluorophores between 450 and 900 nm. Primary tumor and lung specimens were imaged immediately after necropsy using a fluorescence microscope (Leica Microsystems, Bannockburn, IL).

Microscopy, histological, and immunohistochemical analysis

Cultured cells and stained and immunohistochemical tissue sections were photographed using an Olympus BX41 microscope and an Olympus Q COLOR 5 photo camera (Olympus Corp., Lake Success, NY). Tissue specimens were fixed with 10% buffered formalin phosphate immediately after necropsy and embedded in paraffin blocks. Sections of the dissected orthotopic thyroid tumor were hematoxylin and eosin stained before histopathologic evaluation by an endocrine pathologist (P.M.S.). Sections of formalin-fixed tissues were also processed for immunohistochemical analysis as previously described (10). Immunohistochemical analysis was performed using thyroid transcription factor 1 (TTF-1; Dako, Carpinteria, CA), B220 (BD Pharmingen, San Jose, CA), CD3, CD8, and CD163 (Leica Microsystems) antibodies.

Western blot analysis

Whole cell lysates were obtained by lysing cultured cells in plates with RIPA buffer, separated by sodium dodecyl sulfate polyacrylamide gel electrophoresis, transferred to nitrocellulose membranes, and ultimately probed with antibodies against ERK, phosphorylated ERK, AKT, phosphorylated AKT, PTEN, TTF-1, E-cadherin, N-cadherin, and tubulin (Cell Signaling Technologies, Beverly, MA) diluted 1:1000 in Tris-buffered saline with TWEEN containing either 5% milk or bovine serum albumin. Horseradish peroxidase-conjugated secondary antibodies (Cell Signaling Technologies) were then used, and the membranes were treated with a peroxidase substrate for enhanced chemiluminescence (Thermo Scientific, Rockford, IL) before film exposure.

Cellular growth rate curve

For each cell line, 2.5×10^4 cells were seeded in triplicate in a 12-well plate and allowed to adhere overnight. The following day (day 0) and at days 2, 4, and 6, cells were washed with phosphate-buffered saline, fixed with 10% formalin, and stored at 4°C. The fixed cells were washed with phosphate-buffered saline before staining with 0.1% crystal violet in 20% methanol. After washing with water, the cells were dried and 1 mL of 10% acetic acid was added to each well. The absorbance at 595 nm was analyzed for each line and time point.

Results

The MAPK and PI3K-AKT signaling pathways are active in $BRAF^{V600E}$-positive thyroid cancer cell lines derived from genetically engineered mouse models of PTC and ATC

We characterized four distinct murine thyroid cancer cell lines derived from tumors that developed in genetically engineered models of PTC and ATC. These cell lines were derived from genetically engineered mice with alterations in *Braf*, *p53*, and *Pten*, genes known to play an important role in aggressive thyroid cancer (5). The cell lines are listed as TBP-3868, TBP-3743, TBPt-3403, and TBPt-3610R (Table 1). In brief and to be published elsewhere, the genetically engineered mice received tamoxifen to induce thyroid-specific expression of Cre recombinase and consequent recombination and expression of $Braf^{V600E}$ from the endogenous *Braf* promoter in the thyroid gland. Additionally, these mice were homozygous for either *p53* or *Pten* floxed alleles, and the tamoxifen-induced expression of Cre resulted in tissue-specific deletions at these loci in the thyroid gland. The established TBP and TBPt cell lines were named to reflect their derivation from tumors arising in either ***T****PO*Cre^{ER}; ***B****raf*$^{tm1Mmcm/WT}$; *Tr****p****53*$^{tm1Brn/tm1Brn}$ (TBP) or ***T****PO*Cre^{ER}; ***B****raf*$^{tm1Mmcm/WT}$; ***Pt****en*$^{tm1Hwu/tm1Hwu}$ (TBPt) mice (Fig. 1). Phosphorylated ERK, indicative of activated MAPK signaling, was detected by Western blot analysis of each of the murine thyroid cancer cell lines at levels comparable to those in the $BRAF^{V600E}$-positive human ATC cell line, 8505c (Fig. 2A). Loss of PTEN protein expression was evident in the *Pten*-deleted lines, TBPt-3403 and TBPt-3610R, and consequently elevated levels of phosphorylated AKT were detected. Modest levels of AKT phosphorylation are also detected in TBP-3868, TBP-3743, and the human ATC line 8505c (Fig. 2A). *Bona fide* human thyroid cancer cell lines 8505c and

Table 1. Murine Thyroid Cancer Cell Lines

Cell line	*Type*	*Mutations*	*Genotype*	*TTF-1 staining*	*Tumor volume (mm^3, 4 weeks)*	*Metastasis detected?*	*Immune infiltration*
TBP-3868	PTC	$BRAF^{V600E/WT}$ $p53^{-/-}$	*TPO*-Cre^{ER} *Braf*$^{tm1Mmcm/+}$ *p53*$^{tm1Brn/tm1Brn}$	Focally positive	211	No	CD3, CD8, B220, CD163
TBP-3743	ATC	$BRAF^{V600E/WT}$ $p53^{-/-}$	*TPO*-Cre^{ER} *Braf*$^{tm1Mmcm/+}$ *p53*$^{tm1Brn/tm1Brn}$	Weakly and diffusely positive	390[a]	No	CD3, CD8, B220, CD163
TBPt-3403	ATC	$BRAF^{V600E/WT}$ $PTEN^{-/-}$	*TPO*-Cre^{ER} *Braf*$^{tm1Mmcm/+}$ *Pten*$^{tm1Hwu/\ tm1Hwu}$	Weakly and diffusely positive	34	No	Not tested
TBPt-3610R	ATC	$BRAF^{V600E/WT}$ $PTEN^{-/-}$	*TPO*-Cre^{ER} *Braf*$^{tm1Mmcm/+}$ *Pten*$^{tm1Hwu/\ tm1Hwu}$	Weakly and diffusely positive	134	No	Not tested

[a]Tumor volume measured at 2 weeks.
ATC, anaplastic thyroid cancer; PTC, papillary thyroid cancer.

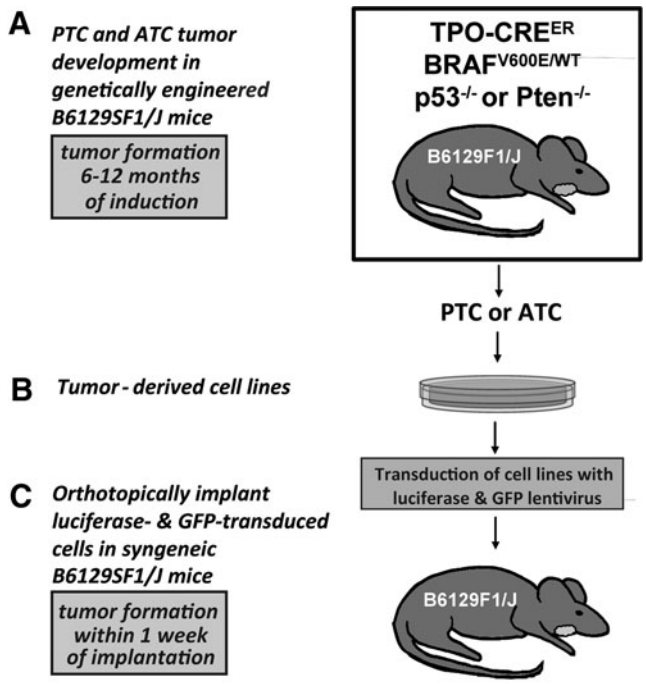

FIG. 1. $BRAF^{V600E}$-postive thyroid cancer cell lines derived from genetically engineered mouse models are orthotopically implanted into syngeneic mice. **(A)** Thyroid tumors developing in the initial genetically engineered mice after the induction of thyroid-specific Cre expression and consequent thyroid-specific recombination and expression of $Braf^{V600E}$ from the endogenous *Braf* promoter in TPOCreER; $Braf^{tm1Mmcm/WT}$ mice (B6129F1/J) with either biallelic *p53* deficiency ($Trp53^{tm1Brn/tm1Brn}$) or *Pten* deficiency ($Pten^{tm1Hwu/tm1Hwu}$). **(B)** Cells were cultured from either a *p53*-deficient tumor with PTC characteristics or ATC tumors arising in the *p53*-deficient and *Pten*-deficient backgrounds. **(C)** After transduction with luciferase and GFP lentivirus, each cell line was surgically implanted into the thyroid bed of syngeneic B6129SF1/J mice. ATC, anaplastic thyroid cancer; PTC, papillary thyroid cancer.

BCPAP express TTF-1 (NKX2-1) as do the TBP and TBPt cell lines, confirming the thyroid origin of each of the murine lines (Fig. 2B). The murine PTC line, TBP-3868, expresses the epithelial marker E-cadherin (CDH1) and low levels of the mesenchymal marker N-cadherin (CDH2), whereas the murine ATC lines lack E-cadherin expression and exhibit higher levels of N-cadherin (Fig. 2B). Interestingly, neither E-cadherin nor N-cadherin is detected in the human PTC line, BCPAP, and the human ATC line, 8505c, shows low N-cadherin only at long exposure (Fig. 2B). The mesenchymal marker vimentin is detected in all of the lines examined (Fig. 2B).

The murine thyroid cancer cell lines exhibit varied cell morphologies and exhibit higher growth rates than human thyroid cancer lines

Each murine cell line examined grew as a monolayer with morphology reflecting the tumor of origin. TBP-3868 was initially derived from a well-differentiated papillary tumor and, consistent with the expression of E-cadherin, continued to exhibit an epithelial growth pattern in culture with cells growing in close association with each other. The murine cell lines derived from anaplastic tumors, TBP-3743, TBPt-3403, and TBPt-3610R, exhibit more mesenchymal-like morphologies and less cohesive growth patterns (Fig. 2C).

Reaching confluence four days postplating, all four of the murine lines grow faster than the human PTC and ATC lines, BCPAP and 8505c, which remained subconfluent six days after plating (Fig. 2D). Though the p53-deficient ATC line, TBP-3743, grows moderately faster than both the PTEN-deficient ATC lines and the PTC line, TBP-3868, the relative growth rates of the murine lines do not markedly vary (Fig. 2D).

Orthotopic tumor implantation results in rapid tumor formation in syngeneic B6129SF1/J mice

One million luciferase- and GFP-labeled mouse tumor cells from each of the lines were implanted into one of the thyroid lobes of the immunocompetent common strain B6129SF1/J mice. The implantation of each cell line resulted in rapid tumor development. Tumor size could be followed *in vivo* using luciferase activity (Fig. 3A) and *ex vivo* using GFP (Fig. 3D). Consistent with luciferase activity

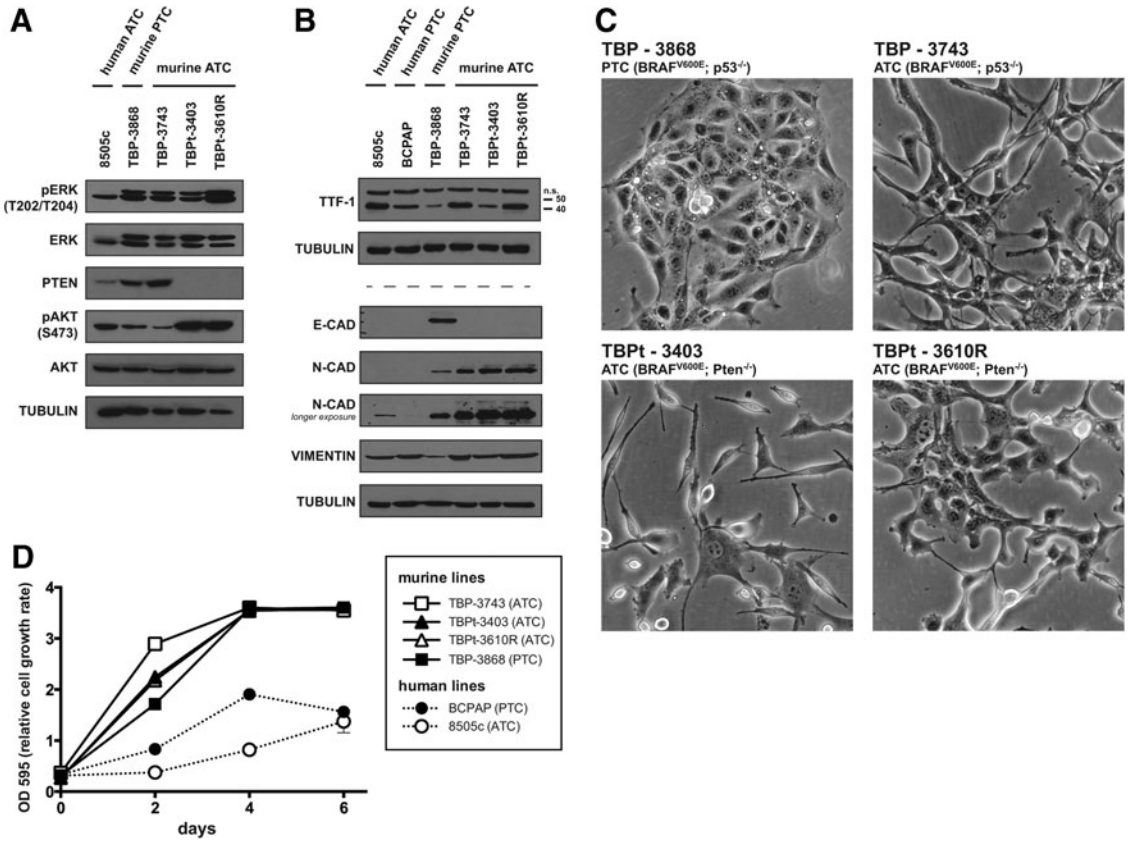

FIG. 2. The murine $BRAF^{V600E}$-postive PTC and ATC cell lines are of thyroid origin, feature active MAPK and PI3K-AKT signaling under basal conditions, and exhibit varied morphologies. **(A)** The phosphorylation status of ERK and AKT was assessed under basal conditions in the immortalized human ATC line, 8505c, and the murine PTC and ATC lines by probing whole cell lysates with antibodies detecting total and phosphorylated levels of ERK and AKT. The absence of PTEN protein expression was verified in the *Pten*-deficient lines, and the levels of phosphorylated AKT were highest in these lines. Whole cell lysates were probed for tubulin to ensure even protein loading. **(B)** The 42 kDa thyroid marker TTF-1 was detected in the human ATC and PTC lines (8505c and BCPAP) as well as in each of the murine cell lines by Western blot analysis. A higher molecular weight nonspecific band was also observed. The epithelial marker E-cadherin was detected in the murine PTC line, TBP-3868. The mesenchymal marker N-cadherin was readily detected in the murine ATC lines and in 8505c and TBP-3868 upon longer exposure. Vimentin was detected in each line examined. Tubulin was individually probed for on the sets of lysates used for TTF-1 and for E-cadherin, N-cadherin, and vimentin as a loading control. **(C)** Each cell line exhibits a unique morphology. 200× magnification. **(D)** Absorbance at 595 nm over time for the murine and human thyroid cancer cell lines. Data are expressed as mean ± standard error of the mean (SEM).

representing actual tumor growth, the greatest level of luciferase activity was observed in mice implanted with the *p53*-deficient ATC line, TBP-3743, at both one and two weeks postimplantation (Fig. 3A). Metastasis to the lungs was not detected during the two- to four-week observation period in any of the cell lines despite the presence of very large and locally aggressive primary tumors (Fig. 3A, D). While direct measurement of the tumor is the most faithful way to determine tumor volume, the correlation between luciferase activity and tumor growth allows live-tracking of tumor growth during experiments while GFP allows visualization of tumor tissue after necropsy (Fig. 3D).

Previously, we and others reported that the implantation of human 8505c ATC cells into SCID mice leads to the formation of thyroid tumors (60–250 mm^3) within four to five weeks postimplantation (9,10,20,21). The growth curves of the murine Pten-deficient lines (TBPt-3403 and TBPt-3610R) are approximately equivalent to those of the human ATC line, 8505c, with tumors reaching the sizes of 34–134 mm^3 one month after implantation. The implantation of the most aggressive murine line examined, TBP-3743, which has both a *BRAF* and *p53* mutation, leads to the formation of large tumors within one week after implantation with mice becoming moribund and requiring euthanasia approximately two weeks postimplantation. Tumors arising from the only murine PTC cell line, TBP-3868, show well-differentiated pathology with clear-cut papillary architecture but with an aggressive *in vivo* growth pattern and achieve volumes similar to those of the TBPt lines one month postimplantation. It is notable that this line, which was derived from a papillary thyroid tumor, recapitulates the architectural characteristics of this tumor subtype after implantation.

The unique *in vivo* growth characteristics and histologic profile of each implanted cell line is described below.

TBP-3868: PTC cell line ($Braf^{V600E/WT}$ and $p53^{-/-}$). TBP-3868 cells developed into well-differentiated PTCs with distinct papillary architecture featuring serrated follicular formation on pathologic examination. The mean tumor volume was 21 mm^3 at one week, and by four weeks postimplantation

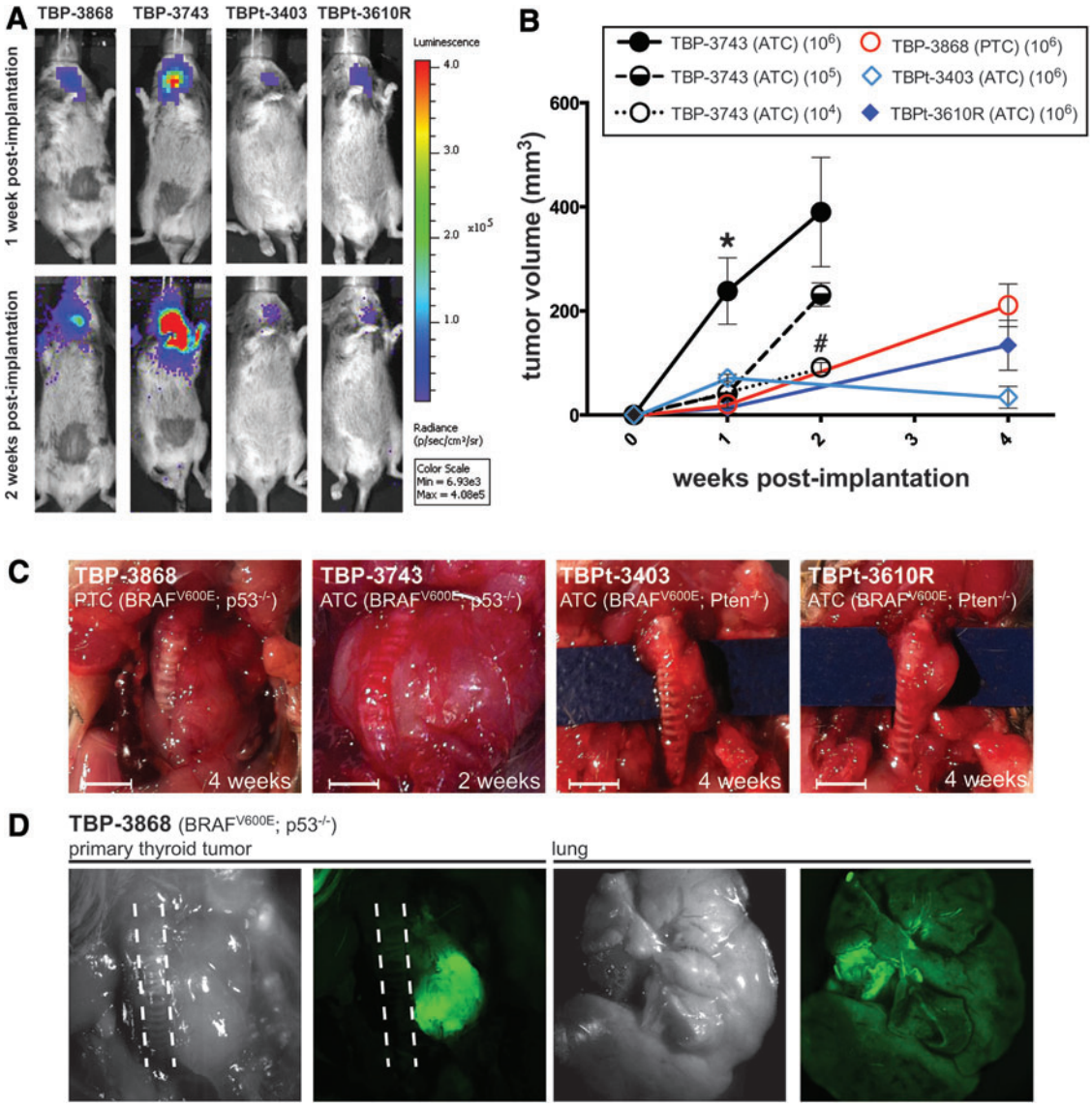

FIG. 3. Thyroid tumors form within one week of orthotopic implantation of PTC and ATC cell lines in syngeneic mice. **(A)** Luciferase activity indicates the proliferation and take of each of the four injected mouse cell lines one week postimplantation. Mice implanted with TBP-3743 exhibit the highest signal (photons/sec). **(B)** Mice were implanted with 10^6 cells of each line and euthanized at one ($n=3$ for each line), two ($n=2$), and four ($n=2$–4) weeks postimplantation. Mice implanted with either 10^4 ($n=2$) or 10^5 ($n=9$) TBP-3743 cells developed tumors and were euthanized two weeks postimplantation. Tumors were measured directly. The TBP-3743 line showed the most aggressive growth *in vivo*. Data are expressed as mean ± SEM and were analyzed by one-way analysis of variance followed by the Tukey multiple comparison test. $^*p<0.05$ of TBP-3743 (10^6 cells) relative to the other lines at one week postimplantation of 10^6 cells. $^\#p<0.01$ of TBP-3743 (10^4 cells) relative to TBP-3743 (10^6 cells) two weeks postimplantation. **(C)** Gross morphology after euthanization at two to four weeks postimplantation of 10^6 cells. Scale bar is 25 mm. **(D)** Dissection and visualization of GFP at four weeks postimplantation indicates that the tumor is comprised of the GFP-expressing thyroid cancer cells and that the lungs are clear of metastatic spread. The results shown are of mice implanted with TBP-3868 cells and are representative of the mice implanted with the ATC cell lines. Dashed lines delineate trachea. Color images available online at www.liebertpub.com/thy

the tumor volume had dramatically increased to 211 mm^3 (Fig. 3B, C). Despite the well-differentiated architecture, the nuclei of the cells predominantly exhibit high-grade nuclear morphology with hyperchromasia, marked pleomorphism, and atypia. TTF-1 expression was focally positive in tumors arising from TBP-3868 (Fig. 4).

TBP-3743: ATC cell line (*Braf*$^{V600E/WT}$ and *p53*$^{-/-}$). Mice implanted with the *p53*-deficient ATC cells, TBP-3743, exhibited large palpable neck masses and a significantly larger mean tumor volume, 238 mm^3, one week postimplantation when compared with mice implanted with the other three cell lines (Fig. 3B, C). In fact, tumors grew so rapidly that mice implanted with 10^6 TBP-3743 cells were euthanized two weeks postimplantation, and at necropsy the mean tumor volume was 390 mm^3. To determine if this rapid tumor formation can be reduced by injecting fewer cells, additional mice were implanted with either 10^4 or 10^5 TBP-3743 cells.

After two weeks, the orthotopic implantation of 10^4 and 10^5 cells gave rise to tumors with mean volumes of 92 mm^3 ($n=2$) and 231 mm^3 ($n=9$), respectively (Fig. 3B). Whereas the tumor size in mice implanted with 10^5 cells was not significantly lower than that in mice implanted with 10^6 cells, the implantation of 10^4 cells results in the formation of significantly smaller tumors ($p<0.01$). Further, mice implanted with 10^4 cells did not present with poor body condition two weeks postimplantation and would putatively exhibit increased survival relative to mice implanted with greater numbers of cells had they not been euthanized for tumor measurement. Histology of this *p53*-deficient ATC line, TBP-3743, showed aggressive spindled and epithelioid neoplasms with marked nuclear atypia, pleomorphism, and hyperchromasia. These tumors readily infiltrated skeletal muscle and entrapped normal thyroid follicles (Fig. 4, data not shown). TTF-1 immunostaining of tumors arising from TBP-3743 was weakly and diffusely positive (Fig. 4).

TBPt-3403: ATC cell line (*Braf*$^{V600E/WT}$ and *Pten*$^{-/-}$). The mean volume of tumors arising in mice implanted with TBPt-3403 cells was 72 mm^3 one week after implantation, and though the mean tumor volume was 34 mm^3 four weeks postimplantation, the decrease in size was not significant (Fig. 3B, C). Tumors arising from this line featured mixed spindled and epitheloid morphology characterized by abundant nuclear pleomorphism, hyperchromasia, and nuclear atypia (Fig. 4). Tumors arising from this ATC-derived cell line exhibited weak and diffuse TTF-1-positive immunostaining (Fig. 4).

TBPt-3610R: ATC cell line (*Braf*$^{V600E/WT}$ and *Pten*$^{-/-}$). Tumors arising from TBPt-3610R measured 14 mm^3 one week postimplantation and grew to a mean tumor volume of 134 mm^3 at four weeks postimplantation (Fig. 3B, C). This *Pten*-deficient line also gave rise to lesions featuring mixed spindled and epitheloid morphology and abundant nuclear pleomorphism, hyperchromasia, and nuclear atypia. There was also infiltration of both thyroid gland and skeletal muscle with malignant cells along with a marked inflammatory response with neutrophils and lymphocytes inside the tumors (Fig. 4). TTF-1 immunostaining was weakly and diffusely positive upon pathologic examination (Fig. 4).

Tumors arising from the PTC and ATC lines exhibit immune cell infiltration

To determine if endogenous immune cells infiltrate tumors arising in mice implanted with PTC (TBP-3868) or ATC

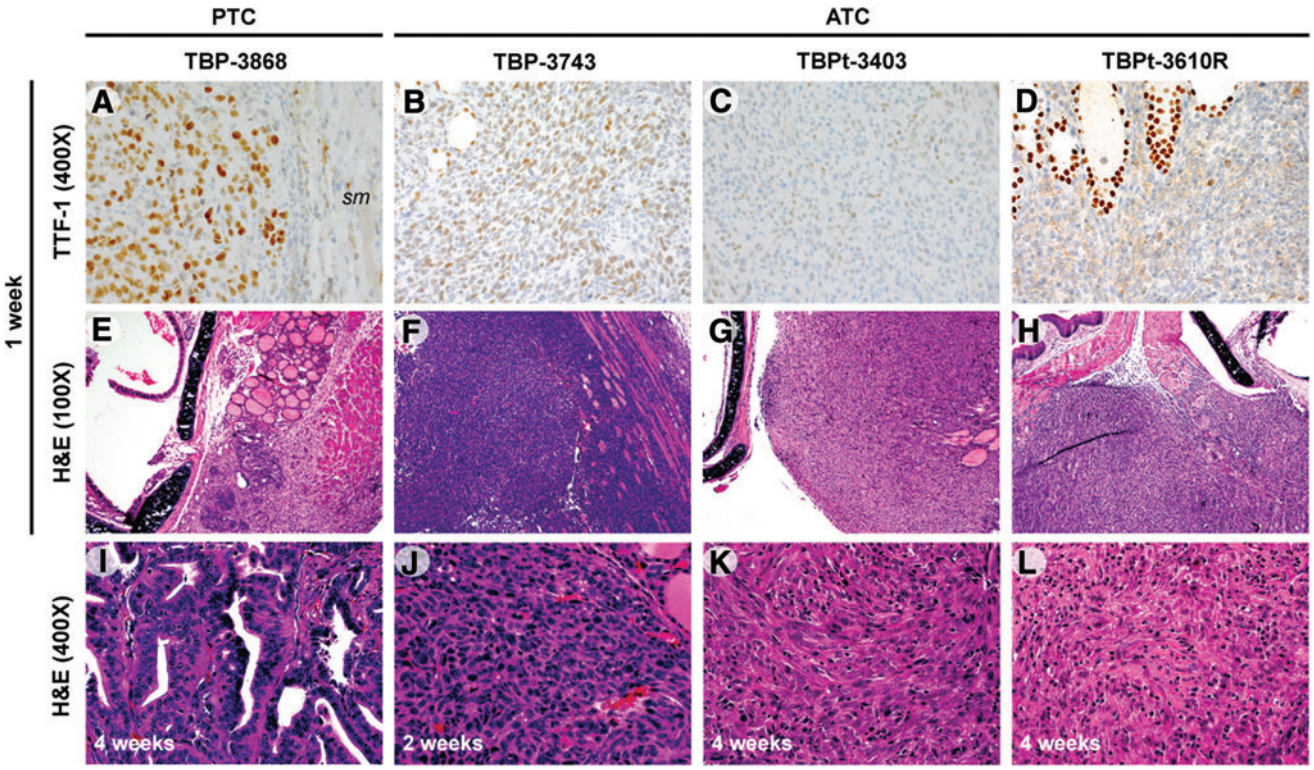

FIG. 4. Histopathologic features indicate the formation of aggressive tumors ranging from well differentiated to anaplastic. **(A–D)** TTF-1 protein expression was detected in sections of tumors established from each line in patterns consistent with the type of tumor of origin. TTF-1 expression is positive in tumors arising from the PTC line TBP-3868 and weakly and diffusely positive in the lines arising from ATC tumors, with strongly positive cells around normal follicles. A region of skeletal muscle (sm), negative for TTF-1, is included in **(A)**. 400× magnification. **(E–H)** H&E staining of tumors one week postimplantation, 100× magnification. **(E)** Well-differentiated papillary thyroid carcinoma in mice implanted with TBP-3868. **(F)** High-grade carcinoma infiltrating skeletal muscle in mice implanted with TBP-3743. **(G)** TBPt-3403 mass entrapping normal thyroid follicles. **(H)** TBPt-3610R showing a single mass with malignant infiltration of skeletal muscle. **(I–L)** H&E staining of tumors two to four weeks postimplantation, 400× magnification. H&E, hematoxylin and eosin; TTF-1, thyroid transcription factor 1. Color images available online at www.liebertpub.com/thy

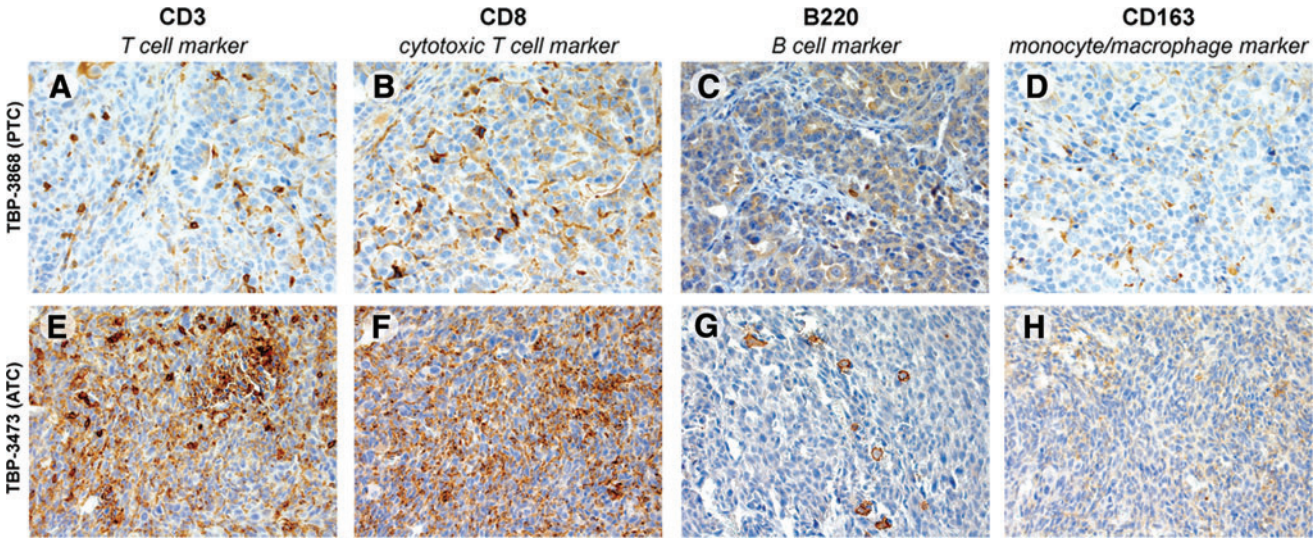

FIG. 5. Immune cell infiltration into TBP-3868 papillary and TBP-3743 anaplastic tumors. **(A–D)** 400× magnification of TBP-3868 PTC tumor four weeks postimplantation, probed with T cell marker CD3 **(A)**, cytotoxic T cell marker CD8 **(B)**, B cell marker B220 **(C)**, and macrophage marker CD163 **(D)**. **(E–H)** 400× magnification of TBP-3743 ATC tumor two weeks postimplantation, probed with T cell marker CD3 **(E)**, cytotoxic T cell marker CD8 **(F)**, B cell marker B220 **(G)**, and macrophage marker CD163 **(H)**. Color images available online at www.liebertpub.com/thy

(TBP-3743) cells, tumor tissue was probed for CD3, CD8, B220, and CD163 to detect T cells, cytotoxic T cells, B cells, and macrophages, respectively. Both the PTC and ATC tumors exhibited abundant CD3+ and CD8+ T cell infiltration (Fig. 5). Though less abundant than the T cells, infiltrating B220+ B cells and CD163+ macrophages were also detected in the TBP-3868 and TBP-3743 tumors (Fig. 5).

Discussion

Here we show that immunocompetent mice implanted with four distinct murine $BRAF^{V600E}$-positive cell lines, TBP-3868, TBP-3743, TBPt-3403, and TBPt-3610R, developed thyroid tumors efficiently, reliably, and within the context of a functional immune system. The genetically engineered mice from which these cell lines were initially derived are the first immunocompetent model of $BRAF^{V600E}$-positive ATC (18). Because of the rapid and simultaneous formation of tumors with known genetic backgrounds, the orthotopic models of $BRAF^{V600E}$-positive PTC and ATC presented herein are highly suitable for investigating novel therapeutics.

While oncogenic BRAF has been implicated in the initiation of PTC, the alteration of additional signaling pathways, including p53 and PI3K-AKT, is believed to be required for progression and dedifferentiation (5,7,22). Thus far, mutations in the thyroid cancer cell lines used in research reflect what grows out in primary culture of tumors and undergoes further alterations when cells are maintained in tissue culture. Our novel methods allow selection of thyroid cancer cell lines with specific genetic alterations in *Braf*, *p53*, and *Pten*. The fact that these cell lines have defined alterations in multiple signaling pathways is invaluable in studying the complex relations between the pathways when it comes to tumor progression, metastasis, or response to drugs. The murine lines used in the novel models presented here are heterozygous for the *Braf* mutation. ($Braf^{V600E/WT}$); thus, in addition to the $BRAF^{V600E}$-positive PTC TBP-3868 tumors, the tumors arising from TBP-3743, TBPt-3403, and TBPt-3610R are the first orthotopic models of ATC to harbor both wild-type and oncogenic *Braf* alleles. As such, the use of these $Braf^{V600E/WT}$ murine thyroid cancer lines will permit investigation into the efficacy of $BRAF^{V600E}$ inhibitors in the context of heterozygous $Braf^{V600E}$. While the clinical significance of $BRAF^{V600E}$ zygosity in the thyroid gland is largely unknown, evidence suggests that $BRAF^{V600E}$ inhibition enhances the tumor immune response of $BRAF^{V600E}$ homozygous melanoma cells but not heterozygous cells (23). Previously reported orthotopic models of PTC and ATC have utilized either PTC cells heterozygous for $BRAF^{V600E}$ (BCPAP) or ATC cells hemizygous for $BRAF^{V600E}$ (8505c) (9,10,20,21). The human ATC line SW1736 is heterozygous for $BRAF^{V600E}$; however, to date, this line has not been orthotopically implanted in mice and the human derivation would prevent implantation in an immunocompetent mouse.

In addition to the expression of oncogenic BRAF, the TBP and TBPt cell lines harbor inactivations of the tumor suppressors *p53* and *Pten*, respectively. We observed a notable difference in growth rate between the tumors with *p53* and *Pten* deletions. Mice implanted with the $BRAF^{V600E}$-positive ATC cell line harboring a biallelic deletion of *p53* (TBP-3743) grow tumors significantly more rapidly than mice implanted with $BRAF^{V600E}$-positive ATC cell lines biallelic for *Pten* deletions (TBPt-3403 and TBPt-3610R). Further, the *p53*-deficient PTC cell line, TBP-3868, gave rise to differentiated tumors that were as large as those arising from the less-differentiated PTEN-deficient ATC cell lines. It is of significant note that the orthotopic tumors recapitulate the histology of the source tumors from which each line was initially derived. Implantation of the TBP-3868 PTC line results in the formation of large but well-differentiated tumors, whereas undifferentiated tumors arise after the

implantation of the ATC lines. While distant metastases were not observed in any of our newly developed orthotopic models within a month of implantation, *in vitro* analysis of the cell lines suggests that PTEN loss may convey a greater migratory capacity than p53 loss (data not shown). This observation may be explained by the commensurate increase of phosphorylated AKT that is observed with a loss of PTEN expression, and putative downstream activation of signaling that increases cellular motility.

Beyond the genetic mutations that alter signaling, the tumor microenvironment and immune milieu modulate thyroid tumorigenesis (12,22,24,25). An advantage of the orthotopic approach to modeling PTC and ATC is the faithful recapitulation of the tumor microenvironment and further, with the syngeneic approach utilized here, the presence of endogenous immune cells and their local cytokines. We detect abundant CD3+ T cell infiltration in tumors arising from TBP-3868 PTC and TBP-3743 ATC cells and, importantly, a large portion of these are CD8+ cytotoxic T cells. Increased tumor-associated macrophage density correlates with poor prognosis in patients with advanced thyroid cancer, and the inhibition of tumor-associated macrophage recruitment attenuates disease progression in an immunocompetent transgenic mouse model of PTC (26,27). Whereas the tumors arising from the ATC line TBP-3743 do not present with abundant CD163+ tumor-associated macrophages, tumors arising from the aggressive but well-differentiated PTC line TBP-3868 exhibit robust monocyte/macrophage infiltration. Additionally, though evidence suggests that inflammatory conditions, including those resulting from Hashimoto's thyroiditis, may promote tumorigenesis, several studies demonstrate that PTC is less advanced in patients with concomitant Hashimoto's thyroiditis and associated lymphocytic infiltration, suggesting that an immune response may attenuate tumor progression (28–30). This duality aside, the immune response to tumorigenesis has emerged as a potential avenue of therapy for solid tumors. Approaches for generating targeted patient-specific T cells for prostate cancer and for modulating T cell activity in melanoma patients have been approved by the Federal Drug Administration (31–33). There is potential to refine these approaches, broaden them to other types of cancer, and develop additional immunotherapies.

Our model is not perfect and there are several caveats that should be noted. For one, the implanted cells are monoclonal and lack the cellular heterogeneity found in human tumors. Further, while our cells harbor well-defined genetically engineered mutations relevant to human thyroid cancer, additional undescribed mutations are most certainly playing a role in both our cell lines and human tumors. Other pertinent differences exist between the described orthotopic mouse model and human tumors, including those pertaining to angiogenesis, the stromal environment, and the functioning of the immune system, though these must be considered for any mouse model of human cancer. With regard to invasion, tumor cell implantation, whether orthotopically or under the skin, creates a wound and therefore may confound the analysis of local invasion through the thyroid capsule. Most of our tumors have very rapid growth, which, while very practical for determining initial efficacy of novel therapeutics and elucidating molecular mechanisms, does not allow study of later events such as metastasis. The slowest growing cell line *in vivo*, TBPt-3403, may not be an accurate representation of rapidly growing and progressing anaplastic thyroid tumor; however, given the relatively slow growth of the primary tumor and the putative longer lifespan of implanted mice, there may be an opportunity for distant metastases to arise at later time points, and therefore this model may warrant further investigation.

Thus far, both the limited number of human thyroid cancer cell lines and the need for implantation into immunodeficient mice have hindered the ability to study the effects of targeted therapies aimed at specific mutated pathways in the context of a normal immune system. We have characterized four novel and distinct mouse PTC and ATC cell lines and demonstrated that implanting these BRAF-mutant cell lines into the thyroid glands of syngeneic immunocompetent B6129SF1/J mice results in rapid tumor formation. We suggest that our new models of aggressive murine thyroid cancer in immunocompetent mice allow for the rapid investigation of potential therapeutics.

Acknowledgments

P.V.B. is a recipient of the Ruth L. Kirschstein National Research Service Award for Individual Postdoctoral Fellows (Parent F32) from the National Institutes of Health and National Cancer Institute. S.P. is funded through the National Institutes of Health, the American College of Surgeons, and the American Thyroid Association. The murine thyroid cancer cell lines were derived from mice generated by D.G.M., recipient of a K08 award from the National Institutes of Health and National Cancer Institute, in the laboratory of T.J. We also thank Derrick Jeon at the Center for Systems Biology at Massachusetts General Hospital for assistance with live imaging and Patricia Della Pelle in the Department of Pathology at Massachusetts General Hospital for histological and immunohistochemical investigations.

Author Disclosure Statement

All authors certify that they have no competing financial interests pertaining to any of the data or statements given in this article.

References

1. Chen AY, Jemal A, Ward EM 2009 Increasing incidence of differentiated thyroid cancer in the United States, 1988–2005. Cancer **115:**3801–3807.
2. National Cancer Institute. Thyroid Cancer. www.cancer.gov/cancertopics/types/thyroid (last accessed on June 3, 2013).
3. Xing J, Liu R, Xing M, Trink B 2011 The BRAFT1799A mutation confers sensitivity of thyroid cancer cells to the BRAFV600E inhibitor PLX4032 (RG7204). Biochem Biophys Res Commun **404:**958–962.
4. Bhaijee F, Nikiforov YE 2011 Molecular analysis of thyroid tumors. Endocr Pathol **22:**126–133.
5. Nikiforov YE, Nikiforova MN 2011 Molecular genetics and diagnosis of thyroid cancer. Nat Rev Endocrinol **7:** 569–580.
6. Nucera C, Goldfarb M, Hodin R, Parangi S 2009 Role of B-Raf(V600E) in differentiated thyroid cancer and preclinical

validation of compounds against B-Raf(V600E). Biochim Biophys Acta **1795:**152–161.
7. Fagin JA, Matsuo K, Karmakar A, Chen DL, Tang SH, Koeffler HP 1993 High prevalence of mutations of the p53 gene in poorly differentiated human thyroid carcinomas. J Clin Invest **91:**179–184.
8. Hou P, Liu D, Shan Y, Hu S, Studeman K, Condouris S, Wang Y, Trink A, El-Naggar AK, Tallini G, Vasko V, Xing M 2007 Genetic alterations and their relationship in the phosphatidylinositol 3-kinase/Akt pathway in thyroid cancer. Clini Cancer Res **13:**1161–1170.
9. Nehs MA, Nagarkatti S, Nucera C, Hodin RA, Parangi S 2010 Thyroidectomy with neoadjuvant PLX4720 extends survival and decreases tumor burden in an orthotopic mouse model of anaplastic thyroid cancer. Surgery **148:**1154–1162; discussion 1162.
10. Nehs MA, Nucera C, Nagarkatti SS, Sadow PM, Morales-Garcia D, Hodin RA, Parangi S 2012 Late intervention with anti-BRAF(V600E) therapy induces tumor regression in an orthotopic mouse model of human anaplastic thyroid cancer. Endocrinology **153:**985–994.
11. Nucera C, Nehs MA, Nagarkatti SS, Sadow PM, Mekel M, Fischer AH, Lin PS, Bollag GE, Lawler J, Hodin RA, Parangi S 2011 Targeting BRAFV600E with PLX4720 displays potent antimigratory and anti-invasive activity in preclinical models of human thyroid cancer. Oncologist **16:**296–309.
12. Nucera C, Porrello A, Antonello ZA, Mekel M, Nehs MA, Giordano TJ, Gerald D, Benjamin LE, Priolo C, Puxeddu E, Finn S, Jarzab B, Hodin RA, Pontecorvi A, Nose V, Lawler J, Parangi S 2010 B-Raf(V600E) and thrombospondin-1 promote thyroid cancer progression. Proc Natl Acad Sci USA **107:**10649–10654.
13. Knauf JA, Ma X, Smith EP, Zhang L, Mitsutake N, Liao XH, Refetoff S, Nikiforov YE, Fagin JA 2005 Targeted expression of BRAFV600E in thyroid cells of transgenic mice results in papillary thyroid cancers that undergo dedifferentiation. Cancer Res **65:**4238–4245.
14. Franco AT, Malaguarnera R, Refetoff S, Liao XH, Lundsmith E, Kimura S, Pritchard C, Marais R, Davies TF, Weinstein LS, Chen M, Rosen N, Ghossein R, Knauf JA, Fagin JA 2011 Thyrotrophin receptor signaling dependence of Braf-induced thyroid tumor initiation in mice. Proc Natl Acad Sci USA **108:**1615–1620.
15. Charles RP, Iezza G, Amendola E, Dankort D, McMahon M 2011 Mutationally activated BRAF(V600E) elicits papillary thyroid cancer in the adult mouse. Cancer Res **71:**3863–3871.
16. Chakravarty D, Santos E, Ryder M, Knauf JA, Liao XH, West BL, Bollag G, Kolesnick R, Thin TH, Rosen N, Zanzonico P, Larson SM, Refetoff S, Ghossein R, Fagin JA 2011 Small-molecule MAPK inhibitors restore radioiodine incorporation in mouse thyroid cancers with conditional BRAF activation. J Clin Invest **121:**4700–4711.
17. Antico Arciuch VG, Russo MA, Dima M, Kang KS, Dasrath F, Liao XH, Refetoff S, Montagna C, Di Cristofano A 2011 Thyrocyte-specific inactivation of p53 and Pten results in anaplastic thyroid carcinomas faithfully recapitulating human tumors. Oncotarget **2:**1109–1126.
18. McFadden DG, Vernon A, Santiago PM, Martinez-McFaline R, Bhutkar A, Crowley DM, McMahon M, Sadow PM, Jacks TE 2014 p53 constrains progression to anaplastic thyroid carcinoma in a Braf-mutant mouse model of papillary thyroid cancer. Proc Natl Acad Sci USA (in press).
19. Tomayko MM, Reynolds CP 1989 Determination of subcutaneous tumor size in athymic (nude) mice. Cancer Chemother Pharmacol **24:**148–154.
20. Chan CM, Jing X, Pike LA, Zhou Q, Lim DJ, Sams SB, Lund GS, Sharma V, Haugen BR, Schweppe RE 2012 Targeted inhibition of Src kinase with dasatinib blocks thyroid cancer growth and metastasis. Clin Cancer Res **18:**3580–3591.
21. Nucera C, Nehs MA, Mekel M, Zhang X, Hodin R, Lawler J, Nose V, Parangi S 2009 A novel orthotopic mouse model of human anaplastic thyroid carcinoma. Thyroid **19:**1077–1084.
22. Xing M 2013 Molecular pathogenesis and mechanisms of thyroid cancer. Nat Rev Cancer **13:**184–199.
23. Sapkota B, Hill CE, Pollack BP 2013 Vemurafenib enhances MHC induction in BRAF homozygous melanoma cells. Oncoimmunology **2:**e22890.
24. Nucera C, Lawler J, Parangi S 2011 BRAF(V600E) and microenvironment in thyroid cancer: a functional link to drive cancer progression. Cancer Res **71:**2417–2422.
25. Liotti F, Visciano C, Melillo RM 2012 Inflammation in thyroid oncogenesis. Am J Cancer Res **2:**286–297.
26. Ryder M, Ghossein RA, Ricarte-Filho JC, Knauf JA, Fagin JA 2008 Increased density of tumor-associated macrophages is associated with decreased survival in advanced thyroid cancer. Endocr Relat Cancer **15:**1069–1074.
27. Ryder M, Gild M, Hohl TM, Pamer E, Knauf J, Ghossein R, Joyce JA, Fagin JA 2013 Genetic and pharmacological targeting of CSF-1/CSF-1R inhibits tumor-associated macrophages and impairs BRAF-induced thyroid cancer progression. PloS One **8:**e54302.
28. Marotta V, Guerra A, Zatelli MC, Uberti ED, Di Stasi V, Faggiano A, Colao A, Vitale M 2013 BRAF mutation positive papillary thyroid carcinoma is less advanced when Hashimoto's thyroiditis lymphocytic infiltration is present. Clin Endocrinol (Oxf) **79:**733–738.
29. Schaffler A, Palitzsch KD, Seiffarth C, Hohne HM, Riedhammer FJ, Hofstadter F, Scholmerich J, Ruschoff J 1998 Coexistent thyroiditis is associated with lower tumour stage in thyroid carcinoma. Eur J Clin Invest **28:**838–844.
30. Konturek A, Barczynski M, Wierzchowski W, Stopa M, Nowak W 2013 Coexistence of papillary thyroid cancer with Hashimoto thyroiditis. Langenbecks Arch Surg **398:**389–394.
31. Graziani G, Tentori L, Navarra P 2012 Ipilimumab: a novel immunostimulatory monoclonal antibody for the treatment of cancer. Pharmacol Res **65:**9–22.
32. Lipson EJ, Drake CG 2011 Ipilimumab: an anti-CTLA-4 antibody for metastatic melanoma. Clin Cancer Res **17:**6958–6962.
33. Kantoff PW, Higano CS, Shore ND, Berger ER, Small EJ, Penson DF, Redfern CH, Ferrari AC, Dreicer R, Sims RB, Xu Y, Frohlich MW, Schellhammer PF 2010 Sipuleucel-T immunotherapy for castration-resistant prostate cancer. N Engl J Med **363:**411–422.

Address correspondence to:
Sareh Parangi, MD
Department of Surgery
Massachusetts General Hospital
Harvard Medical School
Wang ACC 460, 15 Parkman Street
Boston, MA 02115

E-mail: sparangi@partners.org